Acta Cryst. (1989). A**45**, 602-609

Absorption Effect on Borrmann–Lehmann Interference Phenomena

BY MAI ZHENHONG AND ZHAO HONG

Institute of Physics, Academia Sinica, Beijing, China

(*Received* 19 *May* 1988; *accepted* 7 *March* 1989)

Abstract

The Borrmann-Lehmann interference phenomena in the moderate-absorption case ($\mu t = 1{\cdot}6$) have been observed. The effect of absorption on the behaviour of X-ray wave fields in a crystal for Borrmann-Lehmann interference phenomena is discussed in detail based on the X-ray dynamical diffraction theory. A general formula for the spacing of Borrmann-Lehmann fringes is derived. The computer simulation patterns agree well with the experimental topographs.

I. Introduction

In 1963, Borrmann & Lehmann discovered a new X-ray diffraction interference phenomenon which is produced by the interference between the rays direct from the point of incidence of X-rays and the rays *via* reflection at the lateral Bragg surface of a crystal. In the early studies of Borrmann-Lehmann (referred to here as BL) fringes, the diffraction corresponded to the high-absorption case with $\mu t = 18$ (Borrmann & Lehmann, 1963) and $\mu t = 76$ (Lehmann & Borrmann, 1967), μ being the normal X-ray linear absorption coefficient and t the crystal thickness. In 1978, Mai Zhenhong & Lang (personal communication) investigated the interbranch interference effects in the moderate-absorption ($\mu t = 1{\cdot}6$) case. Lang, Kowalski, Makepeace & Moore (1986) did experiments in the low-absorption ($\mu t = 0{\cdot}47$) case with synchrotron radiation of wavelengths 1·5 and 1·0 Å. The experimental results in the moderate-absorption cases show that the fringe patterns are strongly dependent upon the crystal-absorption. The spacing of BL fringes in moderate- and low-absorption cases does not confirm those derived by Borrmann and Lang. In this paper, based on dynamical diffraction theory, we investigate the effect of absorption on the behaviour of X-ray wave fields in a crystal for BL interference phenomena in detail, and derive a general formula for the spacing of BL fringes which is valid for high, moderate and low absorption. Also, the computer simulation patterns agree with the experimental topographs.

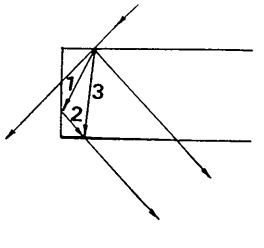

Fig. 1. Scheme of the principle of production of Borrmann-Lehmann interference fringes.

II. The reflection and transmission of the X-ray wave field at the edge of a crystal

In the BL experimental arrangement, a lateral surface of a crystal is located in the Borrmann fan (Fig. 1). When the Poynting vector **s** of a Bloch wave in the crystal impinges upon the lateral surface of the crystal, a significant fraction of its energy is reflected back into the crystal. We then have Laue-Bragg diffraction. Rays may reach the Laue exit surface to the right of the corner B by two paths, one direct from the point of X-ray incidence ([3] in Fig. 1) and the other *via* reflection at the lateral Bragg surface ([1]+[2] in Fig. 1). The optical path difference between these rays produces the BL interference fringes which can be observed in both the K_0 and the K_g beams issuing from the crystal surface to the right of B. Similar to the theoretical treatment of the perfect-crystal case, the wave field inside the crystal is calculated here by plane-wave theory and then by spherical theory.

1. *Plane-wave theory*

Fig. 1 shows the ray paths involved in BL-fringe formation owing to the interference between waves following trajectory [1]+[2] and those following trajectory [3]. When the ray [1] is reflected at R on the lateral surface the boundary conditions of the wave field, allowing for the phase continuity of related fields at the surface, are given by

$$D_0(\mathbf{r}) + D_{0r}(\mathbf{r}) = D_{0t}(\mathbf{r}) \qquad (1a)$$

$$D_g(\mathbf{r}) + D_{gr}(\mathbf{r}) = 0, \qquad (1b)$$

where $D_0(r)$ and $D_g(r)$ are the primary rays inside the crystal excited by the incident beam respectively, $D_{0r}(\mathbf{r})$ and $D_{gr}(\mathbf{r})$ are the rays reflected by the internal lateral surface and $D_{0t}(\mathbf{r})$ is the transmission ray from the lateral surface.

0108-7673/89/090602-08$03.00 © 1989 International Union of Crystallography

$$D_0(\mathbf{r}) = C_0 \exp\{i[(\mathbf{K}\cdot\mathbf{r}_e)+\mathbf{K}_0\cdot(\mathbf{r}-\mathbf{r}_e)]\}$$
$$D_g(\mathbf{r}) = C_g \exp\{i[(\mathbf{K}\cdot\mathbf{r}_e)+\mathbf{K}_g\cdot(\mathbf{r}-\mathbf{r}_e)]\}$$
$$D_{0r}(\mathbf{r}) = C_{0r}\exp\{i[(\mathbf{K}-\mathbf{K}_0)\cdot\mathbf{r}_e + (\mathbf{K}_0-\mathbf{K}_{0r})\cdot\mathbf{r}_s+\mathbf{K}_{0r}\cdot\mathbf{r}]\}$$
$$D_{gr}(\mathbf{r}) = C_{gr}\exp\{i[(\mathbf{K}-\mathbf{K}_g)\cdot\mathbf{r}_g + (\mathbf{K}_g-\mathbf{K}_{gr})\cdot\mathbf{r}_s+\mathbf{K}_{gr}\cdot\mathbf{r}]\}$$
$$D_{0t}(\mathbf{r}) = C_{0t}\exp\{i[(\mathbf{K}-\mathbf{K}_0)\cdot\mathbf{r}_e + (\mathbf{K}_0-\mathbf{K})\cdot\mathbf{r}_s+\mathbf{K}_{0t}\cdot\mathbf{r}]\}.$$

Here $\mathbf{K}$ is the wave vector in vacuum, $\mathbf{K}_0$, $\mathbf{K}_g$, $\mathbf{K}_{0r}$ and $\mathbf{K}_{gr}$ are the wave vectors corresponding to the rays $\mathbf{D}_0$, $\mathbf{D}_g$, $\mathbf{D}_{0r}$ and $\mathbf{D}_{gr}$, respectively. $\mathbf{r}$, $\mathbf{r}_e$ and $\mathbf{r}_s$ are the position vectors of an arbitrary point inside the crystal, on the incident plane and on the lateral surface, respectively.

After calculation, we obtain

$$D_{0r}(\mathbf{r}) = C_{0r}\exp\{i[K_yY+K_zZ - (K\chi_0/2\sin\theta)(\gamma_g/\gamma_0-1) + (K\chi_0/2\gamma_0)t \pm \eta_1(S^2+\bar\beta^2)^{1/2}-\eta_2 S]\} \quad (2a)$$

$$D_{gr}(\mathbf{r}) = C_{gr}\exp\{i[\mathbf{g}\cdot\mathbf{r}+K_yY+K_zZ + (K\chi_0/2\gamma_0)t-(K\chi_0/2\sin\theta) \times(\gamma_g/\gamma_0-1) \pm \eta_1(S^2+\bar\beta^2)^{1/2}-\eta_2 S]\} \quad (2b)$$

$$D_{0t}(\mathbf{r}) = C_{0t}\exp\{i[K_yY+K_zZ - (K\chi_0/2\gamma_0')t_s+(K\chi_0/2\gamma_0)t - (K\chi_0/2\sin\theta)(\gamma_g/\gamma_0-1) \pm \eta_1(S^2+\bar\beta^2)^{1/2}-\eta_2 S]\}, \quad (2c)$$

where

$$C_{0r} = \frac{S\pm(S^2+\bar\beta^2)^{1/2}}{\pm(S^2+\bar\beta^2)^{1/2}}\frac{1}{2}\left(\frac{\gamma_0}{\gamma_g}\right)\left(\frac{\gamma_g''}{\gamma_0''}\right)$$

$$C_{gr} = -C_g = \mp\frac{1}{2}\left(\frac{\chi_g}{\chi_{\bar g}}\right)^{1/2}\left(\frac{\gamma_0}{\gamma_g}\right)^{1/2}\left[\frac{\bar\beta}{(S^2+\bar\beta^2)^{1/2}}\right]$$

$$C_{0t} = \pm\frac{1}{2}\left[\frac{-S\pm(S^2+\bar\beta^2)^{1/2}}{(S^2+\bar\beta^2)^{1/2}}+\frac{\gamma_0}{\gamma_g}\frac{\gamma_g''}{\gamma_0''}\frac{S\pm(S^2+\bar\beta^2)^{1/2}}{(S^2+\bar\beta^2)^{1/2}}\right]$$

$$\eta_1 = \alpha t-\alpha t_s[\gamma_0/\gamma_0''+\gamma_g/\gamma_g'']$$
$$\eta_2 = X-\alpha t+\alpha t_s[\gamma_0/\gamma_0''-\gamma_g/\gamma_g'']$$
$$t_s = (\boldsymbol{\gamma}-\boldsymbol{\gamma}_s)\cdot\mathbf{n}_s$$
$$\mathbf{K}\cdot\mathbf{r} = K_xX+K_yY+K_zZ$$
$$\bar\beta = [KC(\chi_g\chi_{\bar g})^{1/2}/\sin 2\theta_B](\gamma_g/\gamma_0)^{1/2}$$
$$\alpha = \tfrac{1}{2}(\sin 2\theta_B)/\gamma_0$$
$$S = -K_x+(K\chi_0/2\sin 2\theta_B)(1-\gamma_g/\gamma_0)$$

$$\gamma_0' = \cos(\mathbf{n}_s\cdot\mathbf{K}_0) \quad \gamma_g' = \cos(\mathbf{n}_s\cdot\mathbf{K}+\mathbf{g})$$
$$\gamma_0'' = \cos(\mathbf{K}_0\cdot\mathbf{n}_b) \quad \gamma_g'' = \cos(\mathbf{K}_g\cdot\mathbf{n}_b).$$

$\mathbf{r}$ is the position vector of the point of observation and $\mathbf{r}_s$ specifies a point on the lateral surface of the crystal, $\mathbf{n}_s$ is the inwardly directed normal to the lateral surface and $\mathbf{n}_b$ is the outward normal to the exit surface.

2. *Spherical-wave theory*

From the theoretical treatment of Kato (1968) and Saka, Katagawa & Kato (1972), the crystal wave fields are expressed as follows:

Transmitted wave:

$$D_0 = \frac{i}{8\pi^2}\int_{-\infty}^{\infty}\int\frac{1}{K_z}\sum_j^{\alpha,\beta} D_0^j(\mathbf{r})\,dK_x\,dK_y. \quad (3a)$$

Diffracted wave:

$$D_g = \frac{i}{8\pi^2}\int_{-\infty}^{\infty}\int\frac{1}{K_z}\sum_j^{\alpha,\beta} D_g^j(\mathbf{r})\,dK_x\,dK_y \quad (3b)$$

where $D_0^j(\mathbf{r})$ and $D_g^j(\mathbf{r})$ are the wave fields treated by plane-wave theory.

Integrating equation (3), we obtain the wave fields

$$D_{0r} = (i/4)(2\pi Kr)^{-1/2}\exp i(-\pi/4+Kz+\rho)\beta \times(X_{gr}/X_{0r})^{1/2}J_1[\beta(X_{0r}X_{gr})^{1/2}] \quad (4a)$$

$$D_{gr} = \tfrac{1}{4}(2\pi Kr)^{-1/2}\exp i(-\pi/4+Kz+\mathbf{g}\cdot\mathbf{r}+\rho)\beta \times(\chi_g/\chi_{\bar g})^{1/2}J_0[\beta(X_{0r}X_{gr})^{1/2}] \quad (4b)$$

$$D_{0t} = (i/4)(2\pi Kr)^{-1/2}(|\gamma_g''|/\gamma_0'')^{1/2} \times\exp i(-\pi/4+Kz+\rho_t)\beta \times J_1\{\beta[(|\gamma_g''|/\gamma_0'')X_{0r}X_0]\}^{1/2} \quad (4c)$$

where

$$P_t = P-(K\chi_0/2\gamma_0'')t_s,$$
$$P = (K\chi_0/2\gamma_0)[t+(\gamma_0-\gamma_g/\sin 2\theta_B)x],$$

t is the distance from the entrance plane, $X_{0r}=PG$, $X_{gr}=PH$, $X_0=JP$, $X_g=PF$ (Fig. 2).

It is obvious that the amplitudes of the wave fields expressed by equation (4) are very similar to those from a perfect crystal. Therefore the BL fringes could be considered to be an interference phenomenon of wave fields from sources at E and E' (Fig. 2).

3. *Expression for the intensity of the wave field*

From Fig. 2 it can be seen that the BL interference appears in the triangle *RBD*, called the BL region; while the *Pendellösung* interference in the quadrilateral *ERDC* is called the *Pendellösung* region.

In the BL region, the wave fields are expressed by transmitted wave

$$D_0+D_{0r}=(i/4)(2\pi Kr)^{-1/2}\exp i(-\pi/4+Kz+P)\beta \times\{-(X_g/X_0)^{1/2}J_1[\beta(X_0X_g)^{1/2}] +(X_{gr}/X_{0r})^{1/2}J_1[\beta(X_{0r}X_{gr})^{1/2}]\}; \quad (5a)$$

diffracted wave

$$D_g+D_{gr}=-\tfrac{1}{4}(2\pi Kr)^{-1/2} \times\exp i(-\pi/4+Kz+\mathbf{g}\cdot\mathbf{r}+P)\beta(\chi_g/\chi_{\bar{g}})^{1/2} \times\{J_0[\beta(X_0X_g)^{1/2}]-J_0[\beta(X_{0r}X_{gr})^{1/2}]\}, \quad (5b)$$

where $\beta=KC(\chi_g\chi_{\bar{g}})^{1/2}/\sin 2\theta_B$.

In the absorption case, the susceptibilities χ_0, χ_g, $\chi_{\bar{g}}$ and the parameters β and ρ are complex. For symmetric reflection and a centrosymmetric crystal, let

$$\rho_1=\beta(X_0X_g)^{1/2} =\beta\cos\theta[(t\tan\theta)^2-(\eta-a)^2]^{1/2}$$
$$\rho_2=\beta(X_{0r}X_{0g})^{1/2} =\beta\cos\theta[(t\tan\theta)^2-(\eta+a)^2]^{1/2}$$

where $a=AE$ in Fig. 2, η is the position of observation on the exit surface.

In the absorption case, ρ_1 and ρ_2 are complex. For BL experiments in the vicinity of the edge of the crystal,

$$|\rho_1|\gg 1,\ |\rho_2|\gg 1.$$

The intensities of the wave fields can be expressed approximately as follows:

$$I_0=I_{01}+I_{02}+I_{03} =AC\exp(-\mu t/\cos\theta)\{(X_g/X_0)|J_1(\rho_1)|^2 +(X_{gr}/X_{0r})|J_1(\rho_2)|^2-(X_gX_{gr}/X_0X_{0r})^{1/2} \times[J_1^*(\rho_1)J_1(\rho_2)+J_1(\rho_1)J_1^*(\rho_2)]\} \quad (6a)$$

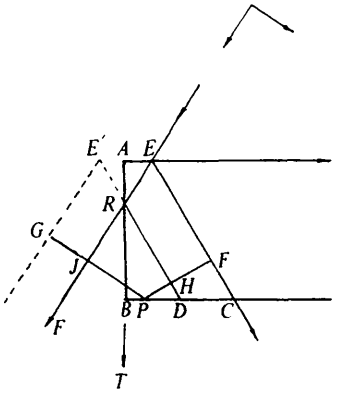

Fig. 2. Scheme of the experimental geometry of Borrmann-Lehmann interference.

$$I_g=I_{g1}+I_{g2}+I_{g3} =AC\exp(-\mu t/\cos\theta)\{|J_0(\rho_1)|^2+|J_0(\rho_2)|^2 -[J_0^*(\rho_1)J_0(\rho_2)+J_0(\rho_1)J_0^*(\rho_2)]\}, \quad (6b)$$

where $A=(32\pi r)^{-1}|\chi_g\chi_{\bar{g}}|/\sin 2\theta$, C is the polarization factor and the symbol * means the complex conjugate. It is seen that the first two terms comprise the *Pendellösung* term and the third term is the BL term.

4. *Behaviour of the interference fringes*

(1) *Diffraction wave.* When ρ_1 and ρ_2 are complex, we have

$$|J_0(\rho)|^2=(\pi|\rho|)^{-1}[\cosh(2\rho^i)+\cos(2\rho^r-\pi/2)] \quad (7)$$

and

$$J_0^*(\rho_1)J_0(\rho_2)+J_0(\rho_1)J_0^*(\rho_2) =\pi^{-1}|\rho_1\rho_2|^{-1/2}[\cosh(\rho_1^i+\rho_2^i)\cos(\rho_1^r-\rho_2^r) +\cosh(\rho_1^r-\rho_2^r)\cos(\rho_1^r+\rho_2^r-\pi/2)]. \quad (8)$$

(*A*) *Pendellösung term.* From equation (7) one can see that the spatial distribution of wave energy has a periodic behaviour that is the well known *Pendellösung* phenomenon. In the low-absorption case ($\mu t<1$), $\rho^i\simeq 0$, $\cosh(2\rho^i)\simeq 1$. Therefore the maximum energy flow is in the margin of the Borrmann fan. This is the margin effect. In the high-absorption case ($\mu t\gg 1$), $\cosh 2\rho^i\gg 1$. Then only one of the waves can penetrate the crystal. This is the anomalous transmission.

(*B*) *BL term.* From (8), one can see that the BL term consists of two parts. Therefore the BL fringes are more complicated than the *Pendellösung* fringes. To simplify the following discussion we call the terms which contain $\cos(\rho_1-\rho_2)$ and those which contain $\cos(\rho_1+\rho_2-\pi/2)$ in (8) 'negative' and 'positive', respectively. Then the fringe spacings of these two terms are expressed by

$$\Delta\eta_\pm=(2\lambda\sin\theta/|\chi_g^r|C)f_\pm(\eta) \quad (9)$$

where

$$f_\pm(\eta)=|(-\{[t\tan\theta/(\eta-a)]^2-1\}^{-1/2} \mp\{[t\tan\theta/(\eta+a)]^2-1\}^{-1/2})^{-1}|. \quad (10)$$

The negative sign is associated with the 'positive' term and the positive sign with the 'negative' term, t is the thickness of the crystal, η is the positional variable on the exit surface of the crystal.

It is easy to see that the spacings of these two terms are different. Their effect on the BL fringe spacing also depends on the intensities of each wave. So when studying the spacing of BL fringes the intensities of wave fields should be considered. Therefore the

absorption effect cannot be neglected. When $(\eta + a) \ll \frac{1}{2}t \tan\theta$, we have:

$$\rho_1^i + \rho_2^i \simeq 2\beta^i t \sin\theta_B$$
$$\rho_1^i - \rho_2^i \simeq 0.$$

For the high-absorption case, $\cosh(\rho_1+\rho_2) \gg \cosh(\rho_1-\rho_2)$. Therefore the spacing of BL fringes is mainly dependent upon the term with negative sign in (9). Then

$$f_-(\eta) \simeq (t\tan\theta)/2a. \qquad (11)$$

Substituting (11) into (9), one can obtain

$$\Delta\eta_- = (\lambda/C|\chi_g^r|)\sin\theta\tan\theta(t/a).$$

This is the formula given by Borrmann & Lehmann (1963).

For the low-absorption case, $\cosh(\rho_1+\rho_2) \simeq \cosh(\rho_1-\rho_2) \simeq 1$. Both 'negative' and 'positive' terms affect the spacing of BL fringes. So, in this case, the spacing of BL fringes is not equidistant, while they are equidistant in the high-absorption case. In the region of $\eta \ll a$, $f_- \ll f_+$. The spacing of BL fringes is dominated by the 'negative' term and modulated by a modulation term. In the region of $\eta > a$ (in our experimental conditions, $BD = t\tan\theta - a > a$), $f_- > f_+$. The fringe spacing is dominated by f_+. It is not constant and decreases with increase in η.

(2) *Transmitted wave.* As a similar treatment to the above

$$|J_1(\rho)|^2 = (\pi|\rho|)^{-1}[\cosh(2\rho^i) + \cos(2\rho^r - 3\pi/2)] \qquad (12)$$

and

$$J_1^*(\rho_1)J_1(\rho_2) + J_1(\rho_1)J_1^*(\rho_2) = (2/\pi)|\rho_1\rho_2|^{-1}[\cosh(\rho_1^i+\rho_2^i)\cos(\rho_1^r-\rho_2^r) + \cosh(\rho_1^i-\rho_2^i)\cos(\rho_1^r+\rho_2^r-3\pi/2)]. \qquad (13)$$

One can see that the effect of absorption in the transmitted wave is similar to that in the diffracted wave. The results mentioned in the section on the diffraction wave are also relevant. In the high-absorption case, the spacing of BL fringes agrees with that given by Borrmann & Lehmann (1963).

Comparing (6*a*) and (6*b*), one finds that the differences between the transmitted wave and the diffracted wave are: (1) the distribution of intensity of the diffracted wave depends on the Bessel function alone while those of the transmitted wave also depends on the coordinate factor, X_g/X_0, X_{gr}/X_{0r}, as well as the Bessel function. Therefore, for the transmitted wave, the distribution of intensity decreases from the direction of the incident beam to that of the reflected beam; (2) the phase difference between the transmitted and diffracted waves is π. Therefore, for the *Pendellösung* fringes, the intensities of transmitted and diffracted waves are complementary. But for the BL fringes, these two waves have a phase difference of π only in the 'positive' term while they have the same phase in the 'negative' term. So in general it is not possible to give a phase difference between them. The conclusion given by Borrmann & Lehmann (1963) is valid only for the high-absorption case.

5. *Results of calculations*

Based on (6), the distributions of intensities of the wave fields both along the exit surface and in the Borrmann fan of specimens were calculated by computer for low, moderate and high absorptions. Figs. 3(*a*) and (*b*) show the distributions of intensities of K_g and K_0 waves along the exit surface of a diamond specimen with $\mu t = 1{\cdot}62$ respectively. It is very clear that in the *Pendellösung*-fringe regions *CD* and *BF* (Fig. 3*b*), the fringes are regular. The intensity oscillations in K_g and K_0 are complementary and the 'beat'

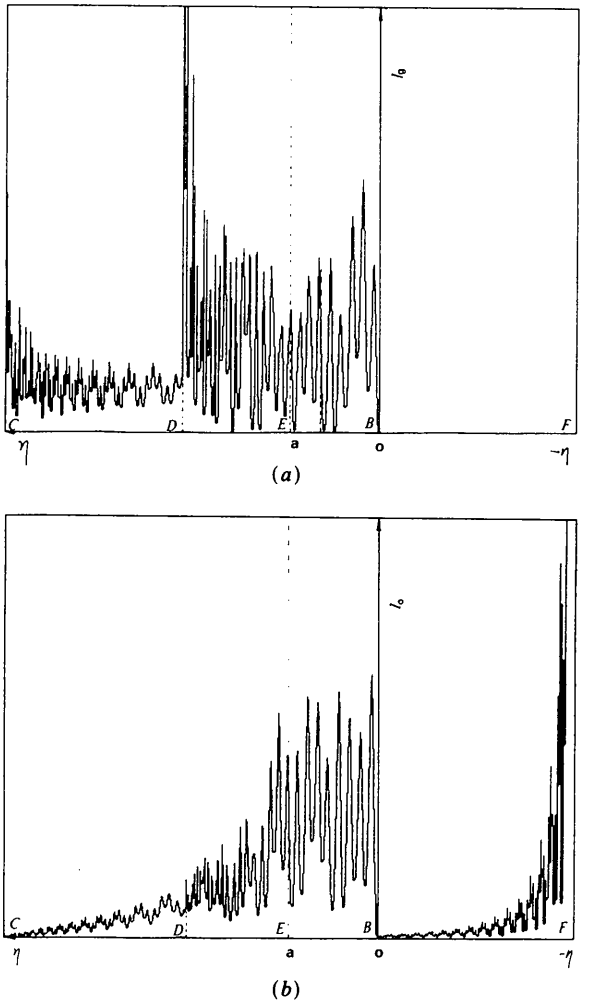

Fig. 3. The distribution of intensities along the exit surface of a diamond specimen, $t = 1$ mm, $\mu t = 1{\cdot}62$, $a = 0{\cdot}24$ mm, Cu $K\alpha_1$ radiation, 220-type reflection. (*a*) K_g beam, (*b*) K_0 beam.

effect is obviously seen owing to the superimposition of the periodicities arising from the superimposition of patterns of the σ- and π-polarization states. In the BL-fringe region, the BL fringes are more complicated. The intensities of K_g and K_0 are not complementary in the region close to the edge of the crystal ($\eta \ll a$). Although the spacing of fringes is approximately constant, the intensities are irregular. In the region far from the edge of the crystal ($\eta \gg a$), the BL fringes emerge irregularly. As the value of η increases, the spacings of fringes decrease.

Figs. 4(a) and (b) show the distributions of intensities of K_g and K_0 waves along the exit surface of a silicon specimen with $\mu t = 18$. One can see that in the high-absorption case the *Pendellösung* fringes disappear and the spacing of the BL fringes is almost constant in the region close to the edge of the crystal. The positions of the maximum and the minimum of intensities of K_g and K_0 along the exit surface are superposed respectively and their intensities decrease as the value of η increases.

Figs. 5(a) and (b) show the distribution of intensities in the Borrmann fan of diamond with $\mu t = 1{\cdot}6$. It is obvious that the *Pendellösung* fringes (*ERDC*) have a hyperbolic shape while the BL fringes (*RBD*) are divergent lines. In Fig. 5(b), one can see the 'beat' effect owing to the superimposition of the patterns of the σ- and π-polarization states.

III. Results of experiment and simulation

To observe the BL interference fringes in the moderate-absorption case ($\mu t = 1{\cdot}6$), a rectangular diamond of $1 \times 2 \times 5$ mm and Cu $K\alpha_1$ radiation were used. Two

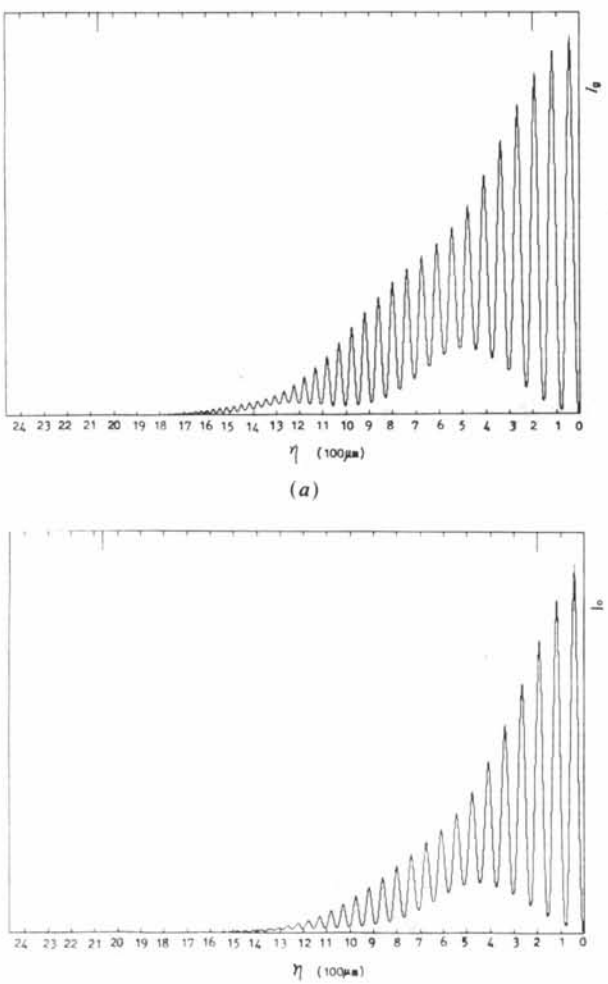

Fig. 4. The distribution of intensities along the exit surface of a silicon specimen, $t = 12$ mm, $\mu t = 18$, $a = 0{\cdot}2$ mm, Cu $K\alpha_1$ radition, 220-type reflection. (a) K_g beam, (b) K_0 beam.

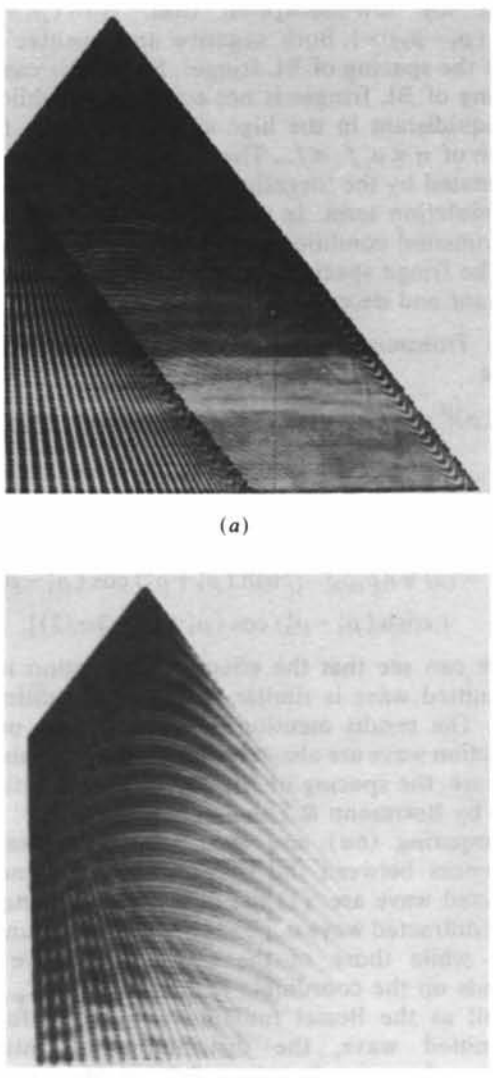

Fig. 5. The distribution of intensities in the Borrmann fan of diamond, $\mu t = 1{\cdot}6$, Cu $K\alpha_1$ radiation, 220-type reflection. (a) σ-polarization state, (b) $\sigma + \pi$-polarization states.

Laue–Bragg situations are considered [shown in Figs. 6(*a*) and (*b*), respectively). Bragg diffracting planes (220) are normal to the major faces of the plate (the 'symmetrical Laue case' for Laue–Laue diffraction). We recorded both the diffracted beam (direction K_g) and the transmitted beam (direction K_0) on photographic plates placed in positions P_g and P_0, respectively. For the recording of the transmitted beam, a screen S was inserted to avoid overexposure of the plate to the direct beam, briefly withdrawing it at the end of the exposure in order to imprint a record of the direct-beam position. An important parameter is the ratio of a, the distance of the point of incidence of X-rays from the edge of the crystal, to t, the crystal thickness. Obviously, Laue–Bragg diffraction conditions only come into play when $(a/t) < \tan\theta$. In our experiment, twelve values of a in the region from 6 to 505 μm were employed, *i.e.* values of a/t in the range 0·006 to 0·5.

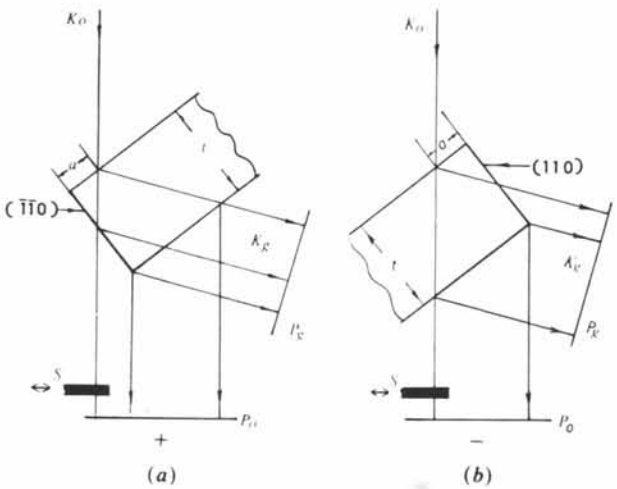

(*a*) (*b*)

Fig. 6. Diffraction geometry for observing BL interference phenomena. (*a*) Negative setting, (*b*) positive setting.

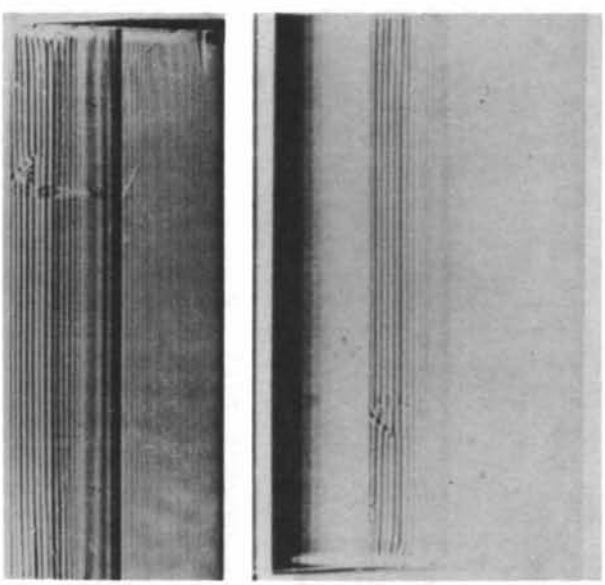

(*a*) 1 2 (*b*)

Fig. 7. Section topographs of diamond showing BL fringes, positive setting, $t = 1$ mm, $\mu t = 1{\cdot}6$, $a = 0{\cdot}24$ mm, Cu $K\alpha_1$ radiation, 220-type reflection. (*a*) K_g-beam image, (*b*) K_0-beam image. The arrows numbered from left to right point to: (1) image of incident beam imprinted by brief removal of screen S; (2) edge of shadow produced by S.

Figs. 7(*a*) and (*b*) are the K_g-beam and K_0-beam patterns, respectively, taken with $a = 0{\cdot}24$ mm positive setting. Borrmann–Lehmann fringes appear in the region *BD* while the *Pendellösung* fringes are observed in the region *CD* and *OF*. In the *Pendellösung* fringes, the intensity oscillations in K_g and K_0 are of course complementary, and a regular 'beat' effect is obviously seen owing to the superimposition of patterns of the σ- and π-polarization states. In BL fringes, the situation of the fringes is more complicated, as expected theoretically. Figs. 8(*a*) and (*b*) are the computer simulations of Figs. 7(*a*) and (*b*), respectively. One can see that the simulation patterns fit the experimental ones well. Figs. 9(*a*) and (*b*) are the section topographs showing BL fringes taken with $a = 0{\cdot}082$ mm, positive setting. Comparison of Fig. 9 with Fig. 7 shows that with decreasing values of a, the spacings of BL fringes increase, but not linearly. Figs. 10(*a*) and (*b*) are the computer simulations of Figs. 9(*a*) and (*b*), respectively. Also the patterns of simulations are in good agreement with experiment. Fig. 11(*a*) is the section topograph showing BL fringes taken with synchrotron radiation, $\lambda = 1{\cdot}5$ Å, σ-polarization mode (Lang *et al.*, 1986). Fig. 11(*b*) is the computer simulation of (*a*). Since the synchrotron radiation has only one polarization mode, the beat of the *Pendellösung* fringes disappears and the BL fringes are uniform and of equal spacing. In Fig. 11(*a*), it is also found that the BL fringes are seriously distorted by lattice imperfections.

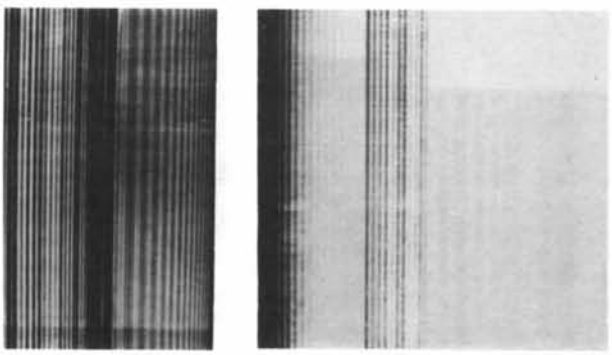

(*a*) (*b*)

Fig. 8. Computer simulation patterns of Fig. 7. (*a*) K_g-beam image, (*b*) K_0-beam image.

Table 1. *Comparison of spacings of Borrmann–Lehmann fringes*

Authors	Diffraction	Radiation	Polarization mode	Beam type	t (mm)	a (mm)	μt	d obs. (μm)	d cal. (μm)	d BL (μm)
Mai	Diamond 220	Cu $K\alpha_1$	$\sigma+\pi$	G	1	0·24	1·6	26·3	28·2	42
Mai	Diamond 220	Cu $K\alpha_1$	$\sigma+\pi$	0	1	0·24	1·6	26·3	28·2	42
Mai	Diamond 220	Cu $K\alpha_1$	$\sigma+\pi$	G	1	0·082	1·6	78	79	122
Mai	Diamond 220	Cu $K\alpha_1$	$\sigma+\pi$	0	1	0·082	1·6	78	79	122
Lang	Diamond 220	Cu $K\alpha_1$	$\sigma+\pi$	G	1	0·38	1·6	13·9	12	26·5
Lang	Diamond 220	Synchrotron (1·5 Å)	σ	G	1	0·44	1·6	11·9	11	22·9
Lang	Diamond 220	Cu $K\alpha_1$	$\sigma+\pi$	G	1	0·21	1·6	29·1	33·5	48
Lang	Diamond 220	Synchrotron (1·5 Å)	σ	G	1	0·20	1·6	29·1	35	46
BL	Si 220	Mo $K\alpha_1$	$\sigma+\pi$	0	12	0·2	18	66	68·5	65
BL	Si 220	Mo $K\alpha_1$	$\sigma+\pi$	G	12	0·2	18	66	68·5	65
BL	Si 220	Mo $K\alpha_1$	$\sigma+\pi$	0	12	0·5	18	33	29·1	30
BL	Si 220	Mo $K\alpha_1$	$\sigma+\pi$	G	12	0·5	18	33	29·1	30

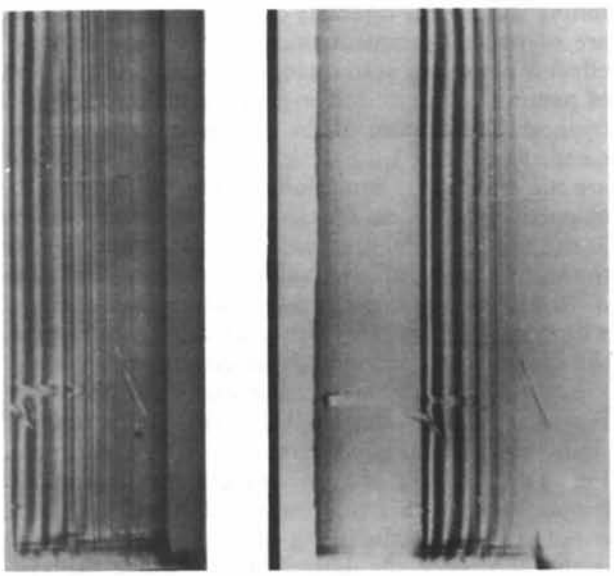

Fig. 9. Section topographs of diamond showing BL fringes, positive setting, $t = 1$ mm, $\mu t = 1{\cdot}6$, $a = 0{\cdot}082$ mm, Cu $K\alpha_1$ radiation 220-type reflection. (*a*) K_g-beam image, (*b*) K_0-beam image The meaning of the numbered arrows is the same as that in Fig 7(*b*).

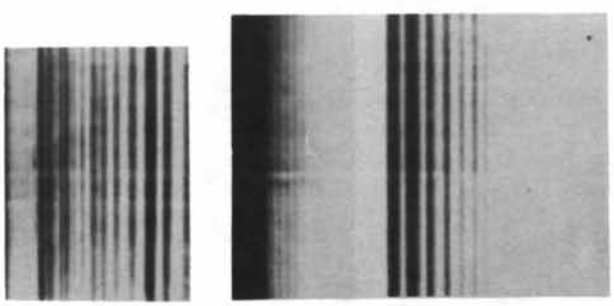

Fig. 10. Computer simulation patterns of Fig. 9. (*a*) K_g-beam image, (*b*) K_0-beam image.

A comparison of the theoretical and experimental data is shown in Table 1. One can see that the spacings calculated, based on our theoretical results, agree with the experimental spacings for all cases; while the data calculated based on the Borrmann formula (Borrmann & Lehmann, 1963) are valid only in the high-absorption case.

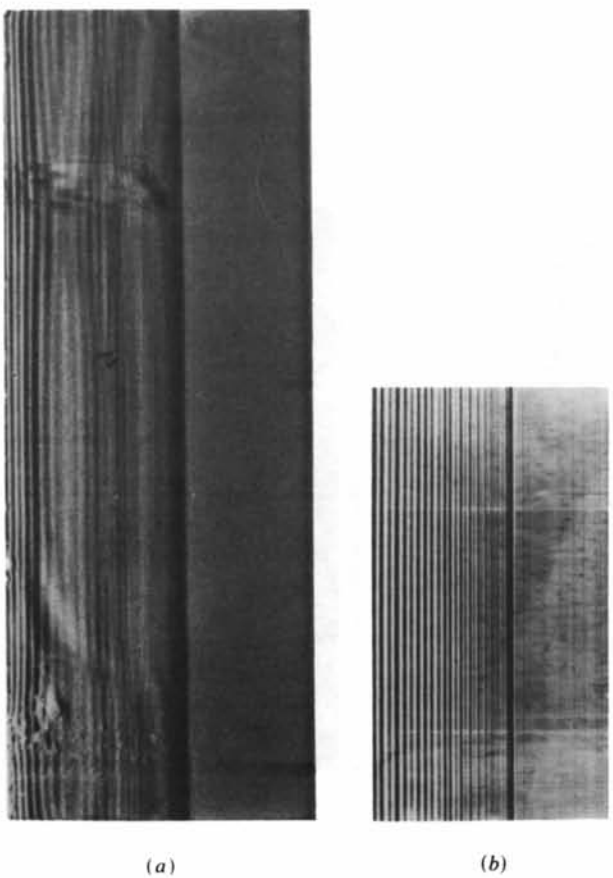

Fig. 11. (*a*) Section topograph of diamond showing BL fringes, synchrotron radiation, $\lambda = 1{\cdot}5$ Å, σ polarization, $a = 0{\cdot}24$ mm, $t = 1$ mm (see Lang *et al.*, 1986, Fig. 7*b*). (*b*) Computer simulation patterns of (*a*).

IV. Concluding remarks

In their pioneer experiments, Borrmann & Lehmann (1963) obtained agreement between observed and calculated fringe spacings within 25% in the high-absorption case and 70% in the low-absorption case. The reason for the deviation is that in their simple theory they considered only the effect of the phase relationship of waves upon the fringe spacing, but neglected the effect of the absorption and the intensities of the waves. In this paper, we have considered all factors affecting the spacings of fringes. Therefore we have obtained good agreement, within 14%, between observed and calculated fringe spacings in the high- and low-absorption cases. The computer simulation patterns also fit the experimental patterns very well. Through our theory the BL fringes are physically clearer.

The authors thank Professor Shun Changde for helpful discussions, the British Council for financial support to MZ and Professor A. R. Lang FRS for guiding advice and topographic facilities at the University of Bristol.

References

BORRMANN, G. & LEHMANN, K. (1963). *Crystallography and Crystal Perfection*, edited by G. N. RAMACHANDRAN, pp. 101-108. London, New York: Academic Press.
KATO, N. (1968) *J. Appl. Phys.* **39**, 2225.
LANG, A. R., KOWALSKI, G., MAKEPEACE, A. P. W. & MOORE, M. (1986). *Acta Cryst.* A**42**, 501-510.
LEHMANN, K. & BORRMANN, G. (1967). *Z. Kristallogr.* **125**, 234-248.
SAKA, T., KATAGAWA, T. & KATO, N. (1972). *Acta Cryst.* A**28**, 102-113, 113-120.

Acta Cryst. (1989). A**45**, 609-613

The Two-Wavelength Technique in Crystal Structure Determination

BY E. A. KLOP, H. KRABBENDAM AND J. KROON

Laboratorium voor Kristal- en Structuurchemie, Rijksuniversiteit, Padualaan 8, 3584 *CH Utrecht, The Netherlands*

(*Received* 24 *January* 1989; *accepted* 23 *March* 1989)

Abstract

A generalization and extension is given of the two-wavelength ratio technique for phase determination [*e.g.* Cascarano, Giacovazzo, Peerdeman & Kroon (1982). *Acta Cryst.* A**38**, 710-720 and references therein]. It is shown that the phase-determining formula of the ratio technique for acentric reflections merely depends on Bijvoet ratios and dispersion terms even if there are no restrictions on these dispersion terms. The system of equations which forms the basis for both the ratio technique and the Bijvoet difference method of Singh & Ramaseshan [*Acta Cryst.* (1968), B**24**, 35-40] (S&R) permits the derivation of a relationship between the scale factors of data collected at different wavelengths for acentric reflections. If this relationship is used as scaling scheme, the S&R method is algebraically equivalent to the ratio technique. For centric reflections the two methods are equivalent provided that the same scaling is applied.

Introduction

The availability of intense tuneable synchrotron radiation has renewed interest in multi-wavelength methods for phase determination of protein structures by means of anomalous X-ray scattering. Two-wavelength methods employ either sums (differences) or ratios of two intensities, called respectively Bijvoet sums (differences) or Bijvoet ratios if the two intensities correspond to Friedel equivalents (or, in general, to reflections which are related by Laue symmetry operations which do not belong to the crystal class).

Singh & Ramaseshan (1968) (S&R) presented an algebraic two-wavelength method using Bijvoet sums and differences which allows calculation of the structure-factor magnitudes of the anomalous scatterers and, after solving the heavy-atom structure, the structure-factor phases. A slightly modified S&R method was used by Klop, Krabbendam & Kroon (1989) together with a direct-methods phasing technique which does not require the solution of the heavy-atom structure.

Unangst, Müller, Müller & Kleinert (1967) proposed an alternative formalism for phase determination when using anomalous-dispersion data which are based on Bijvoet ratios. Their results were derived in a limited form, using an approximation. Geometrical constructions of the multi-wavelength Bijvoet-ratio procedure for phase determination were given by Hosaya (1975). Bartunik (1978) presented an exact two-wavelength Bijvoet-ratio method for phase determination in which the real and imaginary

0108-7673/89/090609-05$03.00 © 1989 International Union of Crystallography